Journal of Power Sources 196 (2011) 428–435

Contents lists available at ScienceDirect

Journal of Power Sources

journal homepage: www.elsevier.com/locate/jpowsour

Ion beam sputter deposition of V_2O_5 thin films

T. Gallasch*, T. Stockhoff, D. Baither, G. Schmitz

Institut für Materialphysik, Westfälische Wilhelms-Universität, Wilhelm-Klemm Str. 10, D-48149 Münster, Germany

ARTICLE INFO

Article history:
Received 6 May 2010
Received in revised form 28 June 2010
Accepted 30 June 2010
Available online 7 July 2010

Keywords:
Ion beam sputter deposition
V_2O_5 thin films
XRD
TEM
EELS
Li intercalation

ABSTRACT

V_2O_5 thin films were deposited by means of dc-ion beam sputtering. To determine the influence of various deposition parameters, samples were characterized by X-ray diffractometry and transmission electron microscopy. Using electron energy loss spectroscopy, the oxidation state of vanadium was quantified based on the chemical shift of absorption edges. Measurement of in-plane direct current showed that the electronic conductivity varies over several orders of magnitude depending on the preparation conditions. The desired structure suitable for battery applications is achieved by sputtering under partial pressure of oxygen and suitable post-annealing under ambient atmosphere. Reversible intercalation of Li into the produced thin films was demonstrated.

© 2010 Elsevier B.V. All rights reserved.

1. Introduction

Vanadium pentoxide is used in a wide range of scientific and technological applications. Electrochromic devices as well as electronic and optical switches are based on V_2O_5. Furthermore the oxide is used as a catalyst for chemical reactions. In addition to $LiCoO_2$ or $LiMn_2O_4$, vanadium oxide is used as electrode material in rechargeable Li-ion batteries and research concentrates on improving the characteristics for the latter application [1–3]. V_2O_5 crystallizes in a layered orthorhombic structure (group: Pmmn) that consists of distorted VO_5 pyramids (unit cell parameters: $a = 11.512$ Å; $b = 3.564$ Å; $c = 4.368$ Å) [4].

The goal of this work is creating this orthorhombic structure in thin film geometry by means of ion beam sputtering aiming at applications in all-solid-state batteries or innovative data storage devices. Although ion beam sputtering is more relevant for fundamental studies rather than industrial production, basic information concerning e.g. structure and microstructure, oxygen and defect concentrations, and Li transport within the thin layers, is of interest for industrial applications and basic research as well.

In contrast to the widely used magnetron technique [5–7], in dc ion beam sputtering a beam of energetic particles, usually neutral Ar, is produced by combining an ion gun with a subsequent neutralizer. This allows growing thin films in a field-free environment so that any charging of target and deposited layers can be reliably avoided which may turn into an important advantage, if thin membranes and electrodes are to be made of materials of low electronic but high ionic conductivity. On the other hand, with the ion beam technique, working pressures are two orders of magnitude lower than in conventional magnetron sputtering (10^{-4} mbar instead of 10^{-2} mbar) and the possibility of using oxygen as sputter gas is restricted. Therefore, achieving stoichiometric contents of oxygen represents a critical issue.

Owing to the described inherent differences between the deposition techniques, structure, microstructure, and properties of produced films may differ significantly. So in general, all important parameters (film thickness, partial pressure of oxygen, substrate temperature during sputtering and, if necessary, post-annealing conditions) have to be carefully optimized.

X-ray diffractometry (XRD) and transmission electron microscopy are carried out in this study to characterize the lattice structure and microstructure of produced films. For a quantitative evaluation of composition and therefore oxidation state of V, electron energy loss spectroscopy (EELS), a very sensitive technique for chemical analysis on smallest length scales, is employed. It will be shown that the EEL spectra depend significantly on preparation parameters. For vanadium oxides all characteristic absorption edges are found in a narrow energy range of only 30 eV, which makes quantification of absolute peak intensities difficult. Therefore, the widely used L_3/L_2 ratio method based on the white line intensities of transition metal compounds [8] is hard to apply, since subtraction of background intensities cannot be performed in a reproducible manner due to peak overlap. As an alternative, Laffont and coworkers suggested measuring the chemical shift of characteristic edges in the energy scale [9]. Most EELS studies of vanadium oxides that have been published yet refer to powder

* Corresponding author. Tel.: +49 0 251 83 33587; fax: +49 0 251 83 38346.
E-mail address: t_gall01@uni-muenster.de (T. Gallasch).

0378-7753/$ – see front matter © 2010 Elsevier B.V. All rights reserved.
doi:10.1016/j.jpowsour.2010.06.099

materials. In this work, a comparative study between powder (acting as reference) and sputter-deposited thin films is given. The analysis is underlined by theoretical calculations [10].

Based on the EELS data, it will be demonstrated that addition of oxygen to the process gas during sputtering and a post-annealing under ambient atmosphere are necessary in order to avoid oxygen deficiencies in the prepared layers.

To complete the extensive sample characterization and to demonstrate the functional efficiency of the thin films working as electrodes, electrochemical investigations such as chrono-potentiometry and cyclic voltammetry (CV) are carried out.

2. Thin film deposition

Thin films of this study were prepared by means of the dc-ion beam sputtering technique. A beam of Ar-ions is produced by electron collisions in an ion gun (Kaufmann type, 40 mm in diameter, delivered by Roth & Rau) and accelerated towards a target with an acceleration voltage of 600 V. Close to the exit grid of the gun, a plasma neutralizer was mounted to discharge the produced beam. Targets (circular discs of 8 cm diameter) were produced by pressing commercial V_2O_5 powder (purity 99.5%, Riedel de Haen). The discs were sintered in air (600 °C, 4 h) to improve mechanical stability. Electronic grade, polished Si(1 1 1) served as substrate for samples dedicated to XRD and TEM characterization. For measurement of electronic conductivity, thin films were deposited upon glass substrates. The film thickness was measured in situ by means of an oscillating quartz balance which was calibrated by comparison to cross-section electron micrographs.Before starting the deposition process, the background pressure of the UHV chamber was always better than 10^{-7} mbar. During deposition, an Ar/O_2 atmosphere was maintained with a total pressure in the order of 10^{-4} mbar and varying oxygen fractions between 5% and 50%. Substrate temperatures were chosen between room temperature and 500 °C controlled to ±5 K by a combination of active water cooling and an UHV compatible hot stage. Subsequent annealing treatments of thin films were performed under ambient atmosphere in a conventional laboratory furnace at 250 °C or 400 °C for up to 3 days. All parameters were carefully controlled in order to generate reproducible conditions in each step of the preparation process.

3. Structural and chemical characterization

3.1. XRD and TEM measurements

XRD measurements were carried out in Bragg-Brentano ($\theta - 2\theta$) geometry (Siemens Kristalloflex, D5000) using Cu K_α radiation (λ = 1.5405 Å). The scanning range was chosen between 10° and 90° for 2θ. For microscopic characterization, electron transparent cross-sections were prepared by grinding and usual ion milling. Prepared cross-sections were investigated by conventional transmission electron microscopy, revealing layer thickness, grain structure and morphology of the interfaces.

Furthermore, electron energy loss spectroscopy (EELS) was used to determine the oxidation state of selected oxide films. As reference, commercial pure powders of VO_2 and V_2O_5 were suspended in anhydrous dimethylcarbonate as suggested in the literature [9]. The suspensions were dropped onto copper TEM-grids coated with a carbon film and dried under ambient atmosphere. Oxide films to be analyzed by EELS were deposited onto identical grids in order to make the comparison as direct as possible. A Zeiss Libra 200 FE microscope, equipped with an in-column energy filter was employed to determine the spectra. The energy resolution of the energy filter amounts to ΔE = 0.7 eV (FWHM of zero loss peak). Since the characteristic energy loss edges (VL_3, VL_2, and O_K) appear all in an energy interval of only 30 eV, quantification based on the usual L_3/L_2 ratio method [8] becomes difficult due to significant peak overlap. Therefore, as an alternative the chemical shift between different edge positions was evaluated as is detailed below.

3.2. Measurements of dc conductivity

Direct current measurements (current-in-plane geometry, CIP) were carried out to determine the electrical characteristics of the thin films. Samples for this measurement were sputtered onto glass substrates of negligible electric conductivity (object slides for optical microscopy). For contact, Pt electrodes of defined geometry were sputter-deposited on top of the oxides. A constant voltage of U = 1 V was applied to a pair of electrodes spaced by about mm and the electronic current was recorded as a function of temperature. The latter was varied in the range between 50 °C and 350 °C.

3.3. Electrochemical measurements

To investigate the electrochemical behavior of sputter-deposited electrodes, chrono-potentiometry and cyclic voltammetry (CV) were carried out. For this, V_2O_5 thin films (120 nm in thickness) were sputter-deposited onto ITO coated glass slides acting as contact material.

In the case of chrono-potentiometry, two identical V_2O_5 electrodes were employed as working as well as reference electrode, while $LiCoO_2$ served as counter electrode acting as Li-donator. The latter was also sputter-deposited from a powder target using a conductive glass slide (ITO covered) as substrate. The described electrodes were dipped into a beaker containing a liquid electrolyte of EC/DMC (1:1) doped with 1 M $LiClO_4$.

For cyclic voltammetry, Li wires served as counter and reference electrodes. To avoid oxidation of Li, the setup was held under inert gas atmosphere using a glove box. Several CV cycles were performed. A scan rate of 1 mV s^{-1} was chosen to investigate the potential range between 1.5 V and 4 V [11].

4. Results and discussion

4.1. Sputtering and XRD

4.1.1. Sputtering under pure Ar

To begin with, sputtering under pure Argon atmosphere at room temperature was studied. Layers of 200–600 nm in thickness were deposited. The resulting films are black colored, which is typical for tetravalent VO_2, whereas a transparent yellow color is expected for V_2O_5. From the respective diffractograms (see Fig. 1a), revealing only the clear reflection of the crystalline Si substrate but no distinguished feature of the produced films, an amorphous structure of the produced layers can be deduced. Second, films of a constant thickness (300 nm) were deposited upon heated Si(1 1 1) substrates in a temperature range of T = 200–500 °C. In addition to the dominating Si signal a slight peak appears which is related to a crystalline VO_2 phase (Fig. 1a).

4.1.2. Sputtering under oxygen partial pressure

To reduce a probable deficit in oxygen, an O_2 partial pressure was added to the gas background inside the deposition chamber to a fraction between 5% and 50% with respect to the total pressure. In contrast to the previous cases, now the color of the deposited films appears to be orange-yellow indicating a substantial increase in oxygen content, but still films of amorphous character are formed (Fig. 1a). Thus, it can be concluded that the desired crystalline orthorhombic V_2O_5 structure cannot be achieved by the applied ion beam sputtering technique without a post treatment, even under

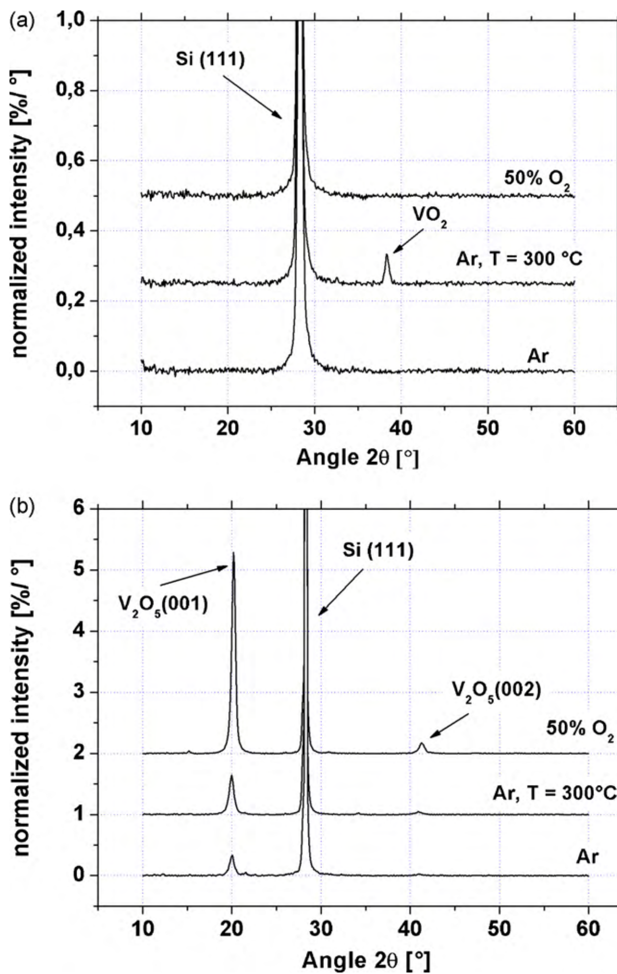

Fig. 1. X-ray diffractograms of (a) as-deposited samples and (b) after post-annealing (400 °C, 3 days). All spectra are normalized to identical integrated intensity allowing the direct quantitative comparison of peak intensities.

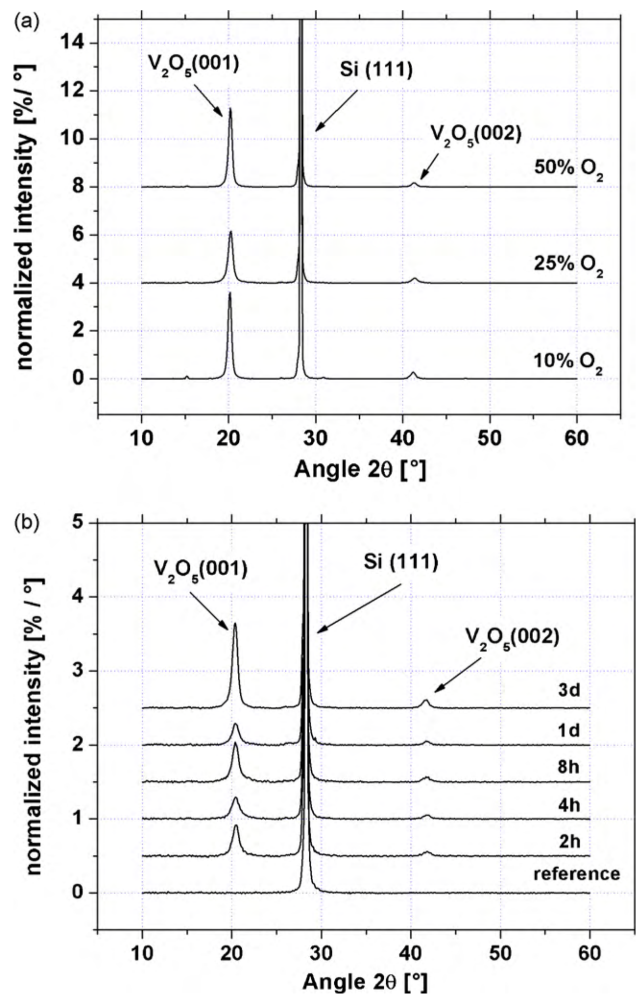

Fig. 2. X-ray diffractograms: (a) after 3 d post-annealing at 400 °C deposited with different partial pressures of oxygen, (b) development of crystalline V_2O_5 during post-annealing at 250 °C under ambient atmosphere (deposition under 10% oxygen).

variation of oxygen content and substrate temperature within the technical applicable range.

4.1.3. Post-annealing treatments

Different samples were post-annealed for 3 days at 400 °C under ambient atmosphere (i.e. about 160 mbar partial pressure of oxygen) to induce crystallization, possibly of the desired orthorhombic lattice structure. Fig. 1a and b compare diffraction spectra of the as-deposited (a) to the annealed states (b) of samples prepared under the discussed different sputtering conditions. Irrespectively of the sputtering conditions, a characteristic V_2O_5 reflection (mostly (0 0 1)) appears after post-annealing in all cases. But as judged from the intensity of the respective peaks, the crystallinity and *c*-axis texture become most clear for samples which were deposited under partial pressure of oxygen (50% O_2). In further experiments, we studied the influence of different oxygen:argon ratios in the deposition atmosphere. The related diffractograms are shown in Fig. 2. Remarkably, it is found that an increase of the oxygen fraction during sputtering has no significant effect. Actually, the sample produced under 10% oxygen shows even slightly higher intensities in the crystalline V_2O_5 reflections than the samples produced under 25% and 50% oxygen.

Finally, we investigated to which extent the annealing treatment may be varied. It is found that a crystalline V_2O_5 phase is already established under the much less demanding annealing of 2 h at 250 °C, see Fig. 2b, which represents an important advantage, if a layer sequence of different materials should be deposited to form e.g. a thin film battery. In complex layer sequences it is important to keep the total thermal budget as low as possible. Former studies [19] showed e.g. that thin films of Li-borate glass may be used as ion-conducting membranes in all-solid-state batteries. In this case however, all deposition and annealing steps must be kept below the respective glass transition temperature which is around 300 °C. We were able to produce vanadium oxide films of reasonable performance under a maximum annealing temperature at 250 °C. Thus, these conditions would be suitable to produce a battery device based on this material combination. In addition the coherent dependence of the data shown in Fig. 2b on annealing conditions emphasizes the reproducibility of the layer deposition technique used in this study.

Table 1 summarizes the peak intensities of all annealed samples in quantitative figures and thus provides information about the degree of thin film crystallinity. In the left columns, the fractions concentrated in the V_2O_5 peaks are stated relative to the total intensity. In calculation of the total intensity, the overwhelming Si(1 1 1) signal caused by the substrate ($2\theta = 27^\circ \ldots 30^\circ$) was excluded, but the diffusive background in between the distinguished peaks caused by amorphous structures was included. In the two further columns at the right, the intensity is always normalized to the respective reference state that is listed in the first line of each of the three data blocks, respectively.

Table 1
V_2O_5 peak intensities in post-annealed samples (400 °C and 3 days, or 250 °C and variable time last data block (indicated by *)). The layer thickness was 300 nm in all cases.

Compare	Sample	$I(001)$ [%]	$I(002)$ [%]	$I_n(001)$	$I_n(002)$
Fig. 1b	Ar	51.0	4.0	1.00	1.00
	Ar, $T = 300$ °C	74.2	5.8	1.99	1.96
	50% O_2	86.3	6.5	7.94	7.67
Fig. 2a	10% O_2	82.4	7.0	1.00	1.00
	25% O_2	78.8	9.2	0.77	0.95
	50% O_2	86.3	6.5	0.92	0.82
Fig. 2b	10% O_2 2 h (*)	73.3	10.2	1.00	1.00
	10% O_2 4 h (*)	62.9	10.4	0.80	0.95
	10% O_2 8 h (*)	67.8	8.4	1.27	1.13
	10% O_2 1 d (*)	64.3	9.7	0.73	0.79
	10% O_2 3 d (*)	80.8	8.9	2.28	1.80

4.2. Electron microscopy

TEM also demonstrates that thin film morphology and crystallinity strongly depend on the parameters used for deposition and post-annealing. In Figs. 3 and 4, a sample deposited under pure Ar atmosphere is compared to a layer which was deposited under oxygen addition (10%) and post-annealed under ambient atmosphere. In the case of sputtering under pure Ar atmosphere the film is mostly amorphous. Only weak spots which can be assigned to both, the tetravalent VO_2 and the desired pentavalent V_2O_5 are detected in the diffraction pattern (Fig. 3b). By contrast, deposition under partial pressure of oxygen and post-annealing under ambient atmosphere leads to a crystalline structure, of which the corresponding reflections are assigned to vanadium pentoxide (Fig. 4b). The grains (20–100 nm in diameter) reveal a globular morphology, no dominating growth direction is observed. In general the TEM measurements are of qualitative character with regard to the degree of crystallinity. For a detailed quantitative evaluation see Table 1 summarizing the XRD results.

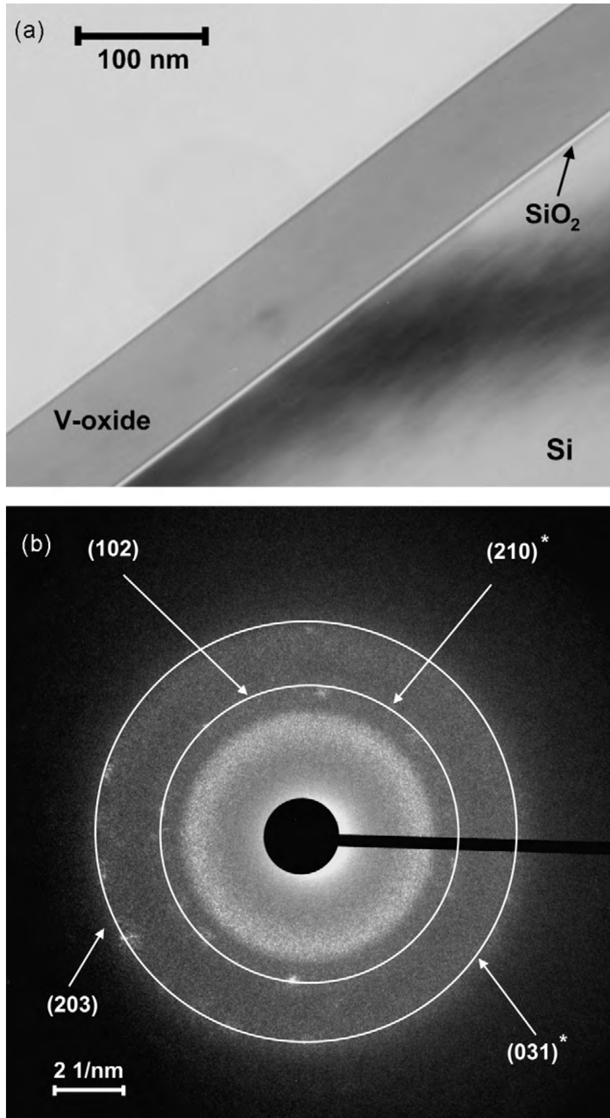

Fig. 3. (a) Vanadium oxide layer (deposited under pure Ar) in bright field, (b) diffraction pattern, possible indices of V_2O_5 and VO_2 are given, the latter marked by *.

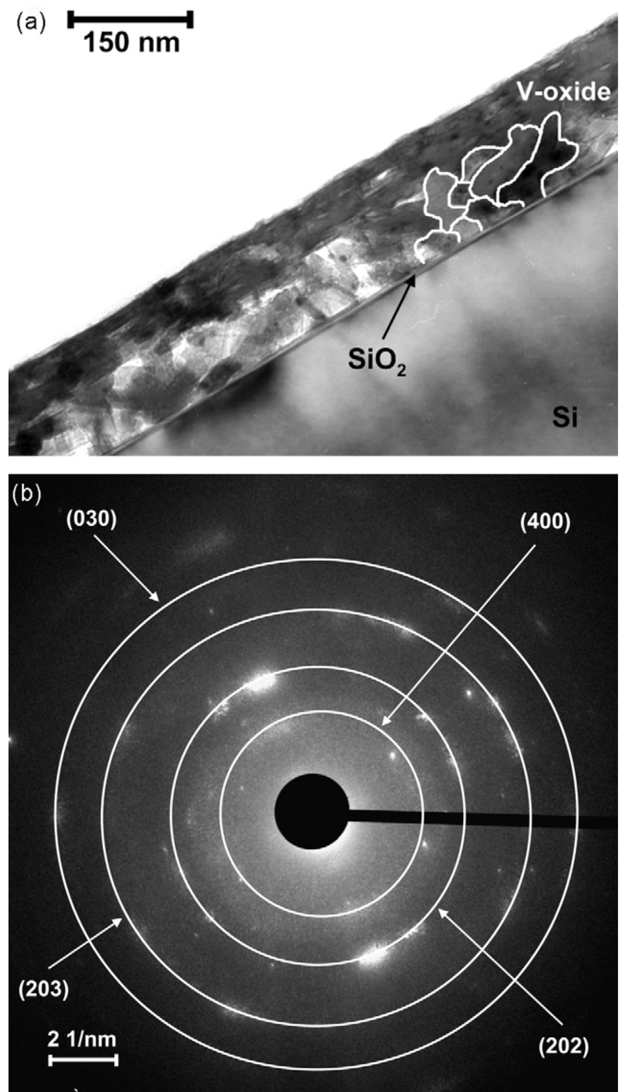

Fig. 4. (a) V_2O_5 layer (10% O_2, post-annealed at 250 °C for 3 d) in bright field, (b) diffraction pattern, a few reflections of V_2O_5 are indexed.

To further characterize the oxidation state of vanadium in dependence on the sputter conditions, EELS was carried out. First, commercial pure powder materials of VO_2 and V_2O_5 were analyzed as reference materials. Fig. 5 presents the observed energy loss spectra of the two powder samples of different, but well known oxidation states.

With increasing oxidation state, the onset of the VL_3 edge is shifted towards higher energy losses. Furthermore, the oxygen signal shows a clear double-peak structure in the case of the pentavalent oxide compared to the only weak double structure in the

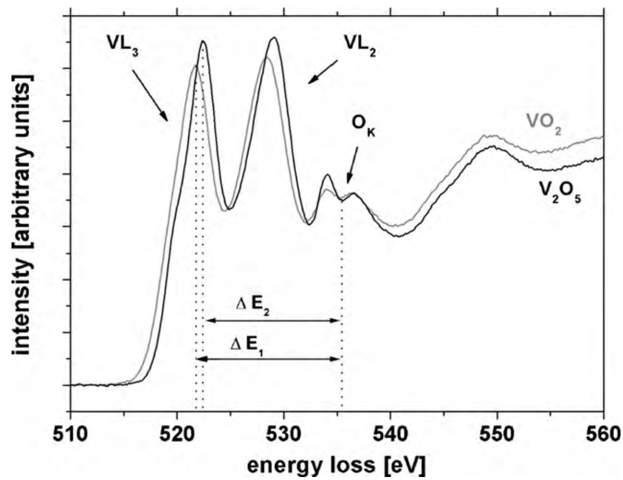

Fig. 5. Background subtracted EEL spectra for VO_2 and V_2O_5 powder samples.

case of VO_2. Similar differences between the EELS of various vanadium oxides are also described in the literature [9] for the bulk case. EEL spectra of the sputter-deposited thin films are presented in Fig. 6. It is clearly seen that the characteristic edges of V shift significantly towards higher values, if oxygen is present during sputtering. The shift gets even more pronounced, if the sample is annealed after deposition. By contrast, the position of the oxygen peak is preserved so that the relative distance between the vanadium and oxygen edges are suggested as a characteristic measure of the chemical shift of the V absorption edges. The corresponding energy intervals are marked by ΔE_i in the figure. Furthermore, it is remarkable that none of the oxygen edges of the sputtered films does reveal a double-peak substructure in obvious contrast to the calibration spectrum of V_2O_5 powder. Interestingly, this feature of missing double edges of oxygen was also reported for the metastable so-called γ-V_2O_5 phase [12], which is distinguished by buckled oxide planes in comparison to the ideal orthorhombic structure. Thus, our EELS data of the deposited thin films suggest, that the lattice structure that has formed by post-annealing of amorphous thin films represents just this metastable modification.As mentioned previously, the characteristic absorption edges of vanadium and oxygen do partly overlap in the tiny energy window of about 30 eV. This hinders the exact determination of peak intensities and therefore prevents the quantification of the ratio between the white lines of

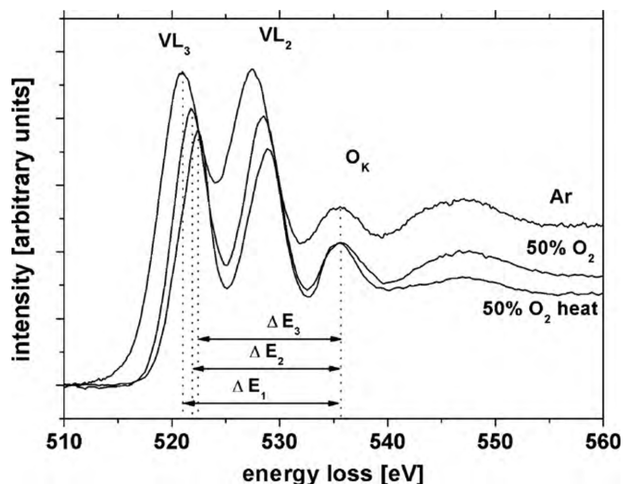

Fig. 6. EELS data of thin films produced under different conditions: sputtered in pure Ar, sputtered in a mixture of Ar/O_2 (1:1), and sputtered in Ar/O_2 (1:1) and subsequently annealed at 400 °C.

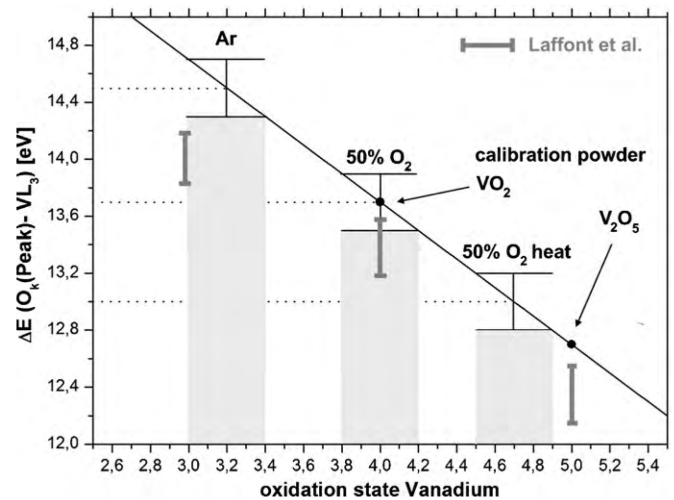

Fig. 7. Quantitative determination of the V-oxidation state in dependence on different sputter parameters, calibration by powder materials. For comparison literature data by Laffont et al. [9] are also shown.

V. Because of this, we chose the shift of the VL_3 edge relative to the O_K peak as a measure of the oxidation state.

The chemical shift of the V edge is a consequence of the redistribution of electrons induced by different electronegativities of vanadium and oxygen. If electronic charge is partly withdrawn from the central vanadium by surrounding oxygen ligands, screening of the positive V nucleus gets less effective and therefore the remaining electron states get stronger bonded to the V atom. In other words, the energy loss due to excitation of one of these electrons from the inner K or L shell increases. A varying oxidation state may be imagined as the central atom (vanadium) being bond to different numbers of identical ligands (oxygen). Based on Kunzl's law dealing with chemical shifts in X-ray absorption near edge spectra (XANES), the shift is a linear function of the so-called coordination charge η of V [13,14].

The constant single bond ionicity I of the vanadium–oxygen bond is given by

$$I = 1 - \exp\left[-\frac{1}{4}(\chi_V - \chi_O)^2\right] = 0.56 \quad (1)$$

in which $\chi_V = 1.63$ and $\chi_O = 3.44$ denote the electronegativites of both partners following Pauling. In combination with the valency Z (i.e. the coordination number) the coordination charge is given by [13]

$$\eta = Z \cdot I \quad (2)$$

so that also a linear dependence of the chemical shift on the average coordination number, meaning the average oxidation state of the V atoms, is expected.

Because of this linearity, a straight line, joining the calibration points of the powder materials (pure VO_2, V_2O_5), is used for quantitative evaluation (see Fig. 7). Having determined the chemical shifts of the sputter-deposited thin films, their oxidation state can be derived directly from the position at this calibration line as demonstrated in the figure. In samples which were sputtered under pure argon, vanadium shows the lowest oxidation state of about +3.2 corresponding to an energy loss distance of about 14.5 eV between VL_3 and O_K. If a significant fraction of oxygen is present during sputtering, this difference decreases and the oxidation state shifts to that of tetravalent oxide, VO_2. But only after the additional annealing treatment, the established oxidation state (+4.7) approaches the ideal one (+5), although still a slight but significant deficit must be stated. Table 2 summarizes the respective quantitative data on the chemical shift and the derived oxidation states. From the compli-

Table 2
Quantitative determination of the V-oxidation state in dependence on different deposition and annealing conditions.

Sample	O_2 peak [eV]	VL_3 peak [eV]	ΔE (O-VL_3) [eV]	V-oxidation state
VO_2 powder	535.4	521.7	13.7	4
V_2O_5 powder	535.1	522.4	12.7	5
Ar	535.6	521.1	14.5	3.2 ± 0.2
50% O_2	535.6	521.9	13.7	4.0 ± 0.2
50% O_2 heat	535.6	522.6	13.0	4.7 ± 0.2

mentary methods diffractometry and analytical microscopy, it can obviously be concluded that ion beam sputtering under optimized conditions is well suited to deposit V_2O_5 films with structure and chemistry very close to the bulk properties.

4.3. Measurement of electronic conductivity

The electronic conductivity has been measured in CIP geometry. In general, an increase of specific conductivity σ with increasing temperature is found, as summarized in Fig. 8. This behavior underlines the semiconducting nature of all samples. Quantitatively the electronic conductivity of the deposited layers strongly depends on the preparation conditions. The highest conductivities together with the lowest activation enthalpies are obtained in the case of sputtering under pure Ar using a heated substrate. Samples sputtered under additional oxygen partial pressure without post-annealing are in the mid-range and the lowest values are obtained in the case of annealed samples (highest activation enthalpy). Samples sputtered at room temperature undergo an amorphous to crystalline transition which is reflected by an increase in conductivity during the first measurement cycle during which the sample is heated to 350 °C.

These experimental observations may be naturally understood by the electronic conductivity of a defective structure: with sputter deposition under pure Ar (and under Ar/O_2 without post-annealing), amorphous films are obtained and the desired stoichiometry is not reached due to a deficit of oxygen. The deficit in oxygen together with the random structure of the network results in the dispersion of lower-valent charge centers (V^{4+}, V^{3+}) which allow a hopping mechanism of the type

$$V^{4+}\text{–O–}V^{5+} \leftrightarrow V^{5+}\text{–O–}V^{4+} \quad (3)$$

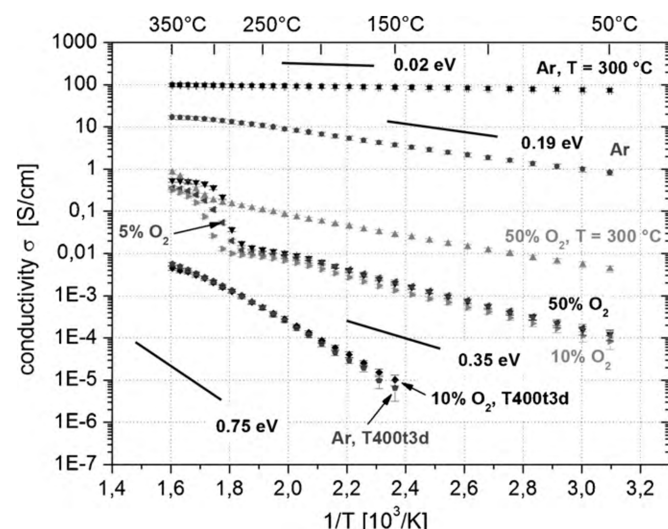

Fig. 8. dc conductivity (first heating cycle) of prepared thin films.

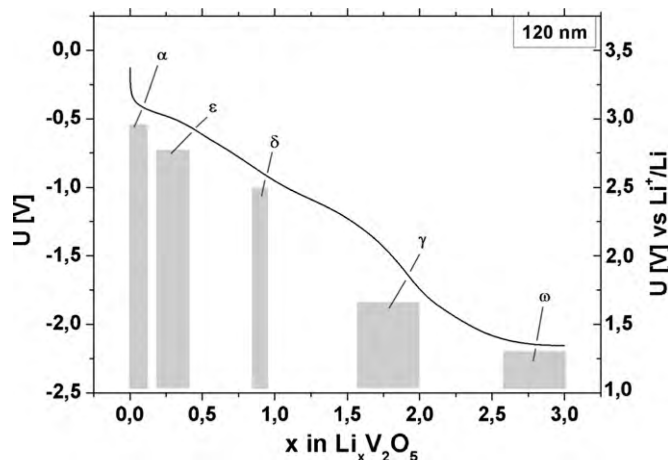

Fig. 9. Chrono-potentiometry (5 μA/cm²) of a 120 nm V_2O_5 thin film produced under optimum conditions. Different $Li_xV_2O_5$ phases are indicated as reported in [18].

for example, leading to a conductivity proportional to the number of oxygen defects [15,16]. Deposited under addition of oxygen to the sputter gas, the samples are still amorphous but the amount of oxygen has increased (as is also indicated by their orange-yellow color) so that the number of possible hopping paths is reduced. In contrast, the annealed crystalline samples are probably better understood as a doped semi-conductor with a clearly defined band gap and localized inter-band states which are easily activated. Thus, the higher the perfection of the structure of the deposited film, the lower is the expected conductivity, since the number of inter-band states gets reduced.

Nabavi et al. prepared amorphous V_2O_5 platelets (a few μm in thickness) by melt spinning [20] resulting in $\sigma = 4 \times 10^{-5}$ S cm^{-1} (at room temperature). Interestingly, this order of magnitude is verified by the thin films of this work sputtered at room temperature under oxygen atmosphere, for which the amorphous structure was proven.

Benmoussa obtains $\sigma = 8.7 \times 10^{-7}$ S cm^{-1} for magnetron sputtered V_2O_5 thin films in optimum structure at room temperature [5]. It is noteworthy that the conductivity of the layers prepared in this work is even less ($\sigma = 2 \times 10^{-9}$ S cm^{-1} at room temperature) after the post-annealing treatment. This suggests that the layers prepared here under optimum conditions are even more perfect.

4.4. Li intercalation

Depending on the amount of Li intercalated into the V_2O_5 material, different compounds based on $Li_xV_2O_5$ are known [17,21]: (i) α-$Li_xV_2O_5$ for $0 \le x \le 0.1$, (ii) ε-$Li_xV_2O_5$ for $0.2 \le x \le 0.4$, (iii) δ-$Li_xV_2O_5$ for $0.9 \le x \le 1.0$. Rocquefelte and coworkers investigated structures with even higher Li concentrations (ζ-phase ($x = 2$) and ω-phase ($x = 3$)) [18].

For electrochemical characterization conventional chrono-potentiometry and cyclic voltammetry (CV) were applied to our thin film electrodes of 120 nm in thickness. A constant current of 5 μA cm^{-2} was applied to investigate insertion of Li with the first method. Variation of the potential with increasing Li content is plotted in Fig. 9. Since V_2O_5 in the as prepared state is used as reference, the initial voltage necessarily amounts to 0 V. However, knowing the equilibrium potential of this reference to Li^+/Li (see results of the CV presented later) the potential axis can be recalculated to the usual Li reference as shown at the right y-axis of the plot. Several "plateaus" in the $U(x)$ dependence indicate two-phase regions of constant chemical potential, while an increased slope of

Table 3
Quantitative evaluation of Li-intercalation processes; * refers to a volume of one stoichiometric unit V_2O_5.

Cycle	Li inserted*	Li extracted*	Li stored*	Charge capacity [μAh cm^{-2} μm^{-1}]	Discharge capacity [μAh cm^{-2} μm^{-1}]
1	3.54	2.32	1.22	88.3	57.8
2	2.79	2.37	0.42	69.9	59.7
3	2.72	2.42	0.30	68.4	60.5
4	2.72	2.47	0.26	68.4	61.6

the function indicates the existence range of a single phase. With this interpretation, the measured curve only coarsely matches the phases reported in the literature [18,21]. It cannot be excluded that phase boundaries may shift in the thin film case due to elastic stress. It is noteworthy that a stoichiometry of $Li_3V_2O_5$, which is also called the ω-phase [18], can be reached.

In order to study reversibility of intercalation, the CV technique is adequate. The first four voltammetric cycles of a vanadium oxide thin film in its optimum structure are shown in Fig. 10a. A voltage range from 1.5 V to 4 V was scanned with a ramp of 1 mV s^{-1} (in technical sense this corresponds to a charge/decharge rate of about 1 C). During the first scan from the open circuit voltage (3.54 V) down to 1.5 V versus Li$^+$/Li, two characteristic cathodic peaks appear at 2.84 V and 2.30 V, which naturally matches to the plateau like two-phase regions in Fig. 9. For later cycles these peaks are broadened but mostly maintain their positions at about 3.0 V and 2.3 V, respectively. Li extraction is represented by an anodic peak at 3.04 V (first scan), which shifts towards higher values and seems to reach 3.3 V as a nearly constant value for the following cycles. As underlined by the EELS measurements, these CV cycles refer to the metastable γ-V_2O_5 phase.

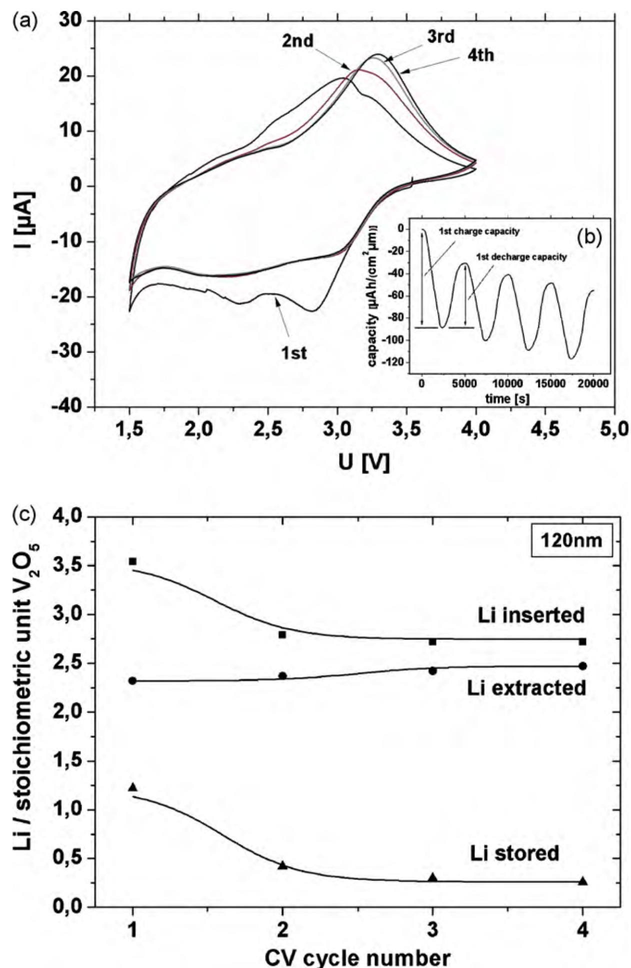

Fig. 10. (a) Cyclic voltammogram of a 120 nm V_2O_5 thin film. The first four cycles are shown. (b) Integrated charge stored in the thin film. (c) Quantitative data of charge and decharge capacities. Difference is presented as loss.

The changes in shape of the voltammograms with increasing cycle number may be due to structural changes induced by Li intercalation. The charges participating are evaluated by integration of the current as presented in Fig. 10b. Clearly, the capacity of the first charging is significantly larger than that of the first decharging which indicates that a considerable amount of Li becomes trapped. The development of capacities during the first few cycles is plotted in Fig. 10c. Clearly, between the amount of inserted and extracted Li a finite difference is seen. However, this difference ("loss") decreases with the cycle number, i.e. the reversibility of Li intercalation improves. After three cycles a loss of about 0.3 Li per stoichiometric unit V_2O_5 is still seen for each cycle. However, this remaining amount seems to saturate. Probably, this saturation loss is due to some side reaction of the electrolyte. Only the higher amounts of Li stored in the material during the first two cycles may correspond to the filling of deep traps in the structure. The initial charge capacity (Li insertion into V_2O_5) amounts to 88 μAh cm^{-2} μm^{-1} and decreases to a constant value of 68 μAh cm^{-2} μm^{-1} for higher cycles (see Fig. 10a). The discharge capacity (Li extraction) even slightly increases with the cycle number and approaches the charging one, which indicates a sufficient reversibility of intercalation.

Table 3 summarizes the measured capacities.

5. Conclusions

In this study, we have demonstrated that V_2O_5 films suitable for battery applications can be produced by dc-ion beam sputtering followed by a post-annealing treatment. The desired layered crystal structure can only be obtained by applying oxygen during the deposition process and additional post-annealing under ambient atmosphere. In order to offer compatible conditions to other components of thin film batteries, the parameters for electrode preparation and post-annealing were optimized to decrease the thermal budget. As a minimum temperature required for post-annealing 250 °C was identified.

The evaluation of chemical shifts in the electron energy loss spectra represents a valuable alternative to the widely used L_3/L_2 method [8] and allows the quantitative determination of oxygen contents and V-oxidation states.

Furthermore, an extensive study of the dc conductivity of the produced thin films was performed, which has verified a semiconducting behavior of the sputter-deposited material. The intercalation function of deposited vanadium oxide thin film electrodes was demonstrated in model electrochemical cells using chrono-potentiometry and cyclic voltammetry. The layers revealed a reversible charge capacity of at least 60 μAh cm^{-2} μm^{-1}.

References

[1] N. Kumagai, et al., Journal of Applied Electrochemistry 28 (1998) 41–48.
[2] M. Levi, et al., Journal of Electroanalytical Chemistry 479 (1999) 12–20.
[3] Y. Wang, G. Cao, Electrochimica Acta 51 (2006) 4865–4872.
[4] R. Enjalbert, J. Galy, Acta Crystallographica C42 (1986) 1467–1469.
[5] M. Benmoussa, et al., Thin Solid Films 265 (1995) 22–28.

[6] C. Navone, J. Pereira-Ramos, Proceedings of the International Workshop: Advanced Techniques for Energy Sources Investigation and Testing, Sofia, 2004, 2004.
[7] A. Gies, et al., Solid State Ionics 176 (2005) 1627–1634.
[8] Z. Wang, et al., Micron 31 (2000) 517–580.
[9] L. Laffont, et al., Micron 37 (2006) 459–464.
[10] C. Hébert, et al., European Physical Journal B 28 (2002) 407–414.
[11] Ch. Reddy, et al., Journal of the Electrochemical Society 155 (8) (2008) A599–A602.
[12] M. Willinger, et al., Physical Review B 69 (155114) (2004) 1–7.
[13] J. Wong, et al., Physical Review B 30 (10) (1984) 5596–5610.
[14] M. Disko, et al., Transmission Electron Energy Loss Spectrometry in Materials Science, The Minerals, Metals & Materials Society, Warrendale, Pennsylvania, USA, 1992.
[15] G. Khan, C. Hogarth, Journal of Materials Science 25 (1990) 5014–5018.
[16] A. Moshfegh, A. Ignatiev, Thin Solid Films 198 (1991) 251–268.
[17] R. Cava, et al., Journal of Solid State Chemistry 65 (1986) 63–71.
[18] X. Rocquefelte, et al., Chemistry of Materials 15 (2003) 1812–1819.
[19] F. Berkemeier, M.R.S. Abouzari, G. Schmitz, Ionics, Springer Verlag, 2008, doi:10.1007/s11581-008-0266-4.
[20] M. Nabavi, et al., Solid State Ionics 28–30 (1988) 1183–1186.
[21] J. Mc Graw, et al., Electrochimica Acta 45 (1999) 187–196.